Orbital order-disorder transition in single-valent manganites

J.-S. Zhou and J. B. Goodenough
Texas Materials Institute, ETC 9.102, University of Texas at Austin, 1 University Station, C2201, Austin, Texas 78712, USA
(Received 21 April 2003; published 3 October 2003)

The temperature dependence of the resistance and the thermoelectric power have been measured to high temperatures on single-crystal $R\mathrm{MnO_3}$ (R=La, Pr, Nd) and $\mathrm{LaMn_{1-x}Ga_xO_3}$ ($0\leqslant x\leqslant 0.5$). The data reveal two well-defined transition temperatures T^* and T_{JT}; at $T<T^*$, a cooperative Jahn-Teller ordering of the occupied e_g orbitals of the $\mathrm{MnO_{6/2}}$ octahedra stabilizes an antiferromagnetic-insulator phase, and at $T>T_{\mathrm{JT}}$, short-range orbital fluctuations stabilize a conductive, ferromagnetic phase. T^* and T_{JT} vary linearly with $\langle\cos^2\phi\rangle$, as does the Néel temperature T_{N}, in the $R\mathrm{MnO_3}$ family where ϕ is the bending of the $(180°-\phi)$ Mn-O-Mn bond angle. All three critical temperatures vary linearly with x in the $\mathrm{LaMn_{1-x}Ga_xO_3}$ systems for $0\leqslant x<0.4$. The phase diagrams for the $R\mathrm{MnO_3}$ and $R\mathrm{NiO_3}$ families show common features; differences in their properties are due to a Hund intra-atomic exchange in $R\mathrm{MnO_3}$ that is not present in $R\mathrm{NiO_3}$ perovskites and to a larger O $2p$ component in the e_g orbitals of the $R\mathrm{NiO_3}$ family.

DOI: 10.1103/PhysRevB.68.144406 PACS number(s): 71.70.Ej, 71.70.Gm, 75.30.−m, 75.30.Et

INTRODUCTION

Perovskites AMO_3 with a tolerance factor $t\equiv(A\text{-O})/\sqrt{2}(M\text{-O})<1$ adjust to the mismatch of their (A-O) and (M-O) equilibrium bond lengths by a cooperative rotation of the $(M\text{-O})_{6/2}$ octahedra. A coopeartive rotation about a cubic [110] axis results in the O orthorhombic phase of $\mathrm{GdFeO_3}$, which has $c/a>\sqrt{2}$. An octahedral-site $M=\mathrm{Mn^{3+}}$ ion has a high-spin $t_{2g}^3e_g^1$ configuration, and a Jahn-Teller distortion of the octahedral site to tetragonal or orthorhombic symmetry lifts the twofold energy degeneracy of the e_g level. In the perovskite $\mathrm{LaMnO_3}$, a cooperative Jahn-Teller distortion of the $\mathrm{MnO_{6/2}}$ octahedra below a temperature T_{JT} orders at long range the occupied e_g orbitals within the (001) planes of an O orthorhombic structure so as to minimize the elastic energy; the orbital ordering produces an O' orthorhombic structure with $c/a<\sqrt{2}$.[1] On heating to $T>T_{\mathrm{JT}}\approx 780$ K, a first-order change from static long-range orbital order to disordered, fluctuating local Jahn-Teller distortions results in a pseudocubic O^*-orthorhombic phase with $c/a\approx\sqrt{2}$.[2]

It has been widely accepted that, in $\mathrm{LaMnO_3}$, the cooperative Jahn-Teller distortion enhances the on-site Coulomb energy U separating the localized-electron $\mathrm{Mn^{4+}/Mn^{3+}}$ and $\mathrm{Mn^{3+}/Mn^{2+}}$ redox energies. On heating through T_{JT}, a decrease in the resistivity and an abrupt drop in the thermoelectric power to a nearly temperature-independent, small value signal a lowering of U to give a partial overlap of the two redox energies.[3] Nevertheless, μ_{eff} does not change on crossing T_{JT},[3] which signals that the electrons remain localized as a result of a strong intra-atomic-exchange coupling (Hund exchange field) between the localized spin $S=3/2$ of the t_{2g}^3 manifold and the mobile e_g electrons. Therefore, the partial overlap of the redox energies has been represented as a fluctuating charge disproportionation $2\mathrm{Mn^{3+}}=\mathrm{Mn^{2+}}+\mathrm{Mn^{4+}}$ on some of the Mn atoms. The disproportionation reaction becomes possible in the orbitally disordered phase where bond-length fluctuations permit breathing-mode as well as Jahn-Teller fluctuations. A change in slope of the temperature dependence of the resistivity $\rho(T)$ and of the thermoelectric power $\alpha(T)$ at $T^*\approx 600$ K is due to nucleation of an orbitally disordered phase in a volume fraction of the high-temperature phase; this volume fraction grows monotonically with increasing temperature in the interval $T^*<T<T_{\mathrm{JT}}$, but it increases discontinuously on heating across T_{JT}. Raman spectroscopy[4,5] has revealed the existence of orbital-disorder fluctuations in the interval $T^*<T<T_{\mathrm{JT}}$.

An abrupt jump in the Weiss constant of the paramagnetic susceptibility on heating through T_{JT} signals a change to three-dimensional (3D) ferromagnetic interactions from the 2D ferromagnetic coupling within (001) planes and antiferromagnetic coupling between these planes (type-A antiferromagnetic order found below a Néel temperature T_{N}) in the O' orthorhombic phase.[3] The existence of real charge transfer in the O^* orthorhombic phase above T_{JT} introduces the possibility of ferromagnetic double-exchange interactions in addition to ferromagnetic vibronic-superexchange interactions.

The proposed vibronic state associated with dynamic Jahn-Teller distortions and real charge transfer above T_{JT} has recently been confirmed by x-ray absorption spectroscopy.[6] Moreover, the spectral weight of optical conductivity moves to lower energy on heating through T_{JT}.[7] However, there is no Drude peak in the optical conductivity, which confirms that the mobile electrons above T_{JT} do not have a momentum described by a well-defined **k** vector as is to be expected for mobile localized electrons.

The electronic state in the O^* orthorhombic phase $T>T_{\mathrm{JT}}$ remains poorly understood, as is evident from these documented data. In this paper, we report the dependence of T^*, T_{JT}, and the transport properties of the $R\mathrm{MnO_3}$ perovskite family, where R is a lanthanide, in order to understand better how these evolve with increasing Mn-O-Mn σ-bond overlap integral. Because the highest overlap integral occurs in $\mathrm{LaMnO_3}$, it is not possible to access by chemical substitution the transition from an orbitally ordered, antiferro-

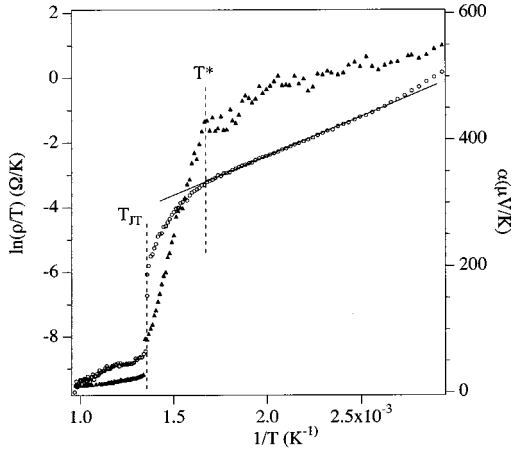

FIG. 1. Resistivity as $\ln(\rho/T)$ and thermoelectric power α versus $1/T$ for single-crystal $LaMnO_3$.

magnetic insulator to a Pauli paramagnetic metal. However, the cooperative Jahn-Teller distortion can be suppressed by diluting Mn^{3+} with a nonmagnetic ion such as Ga^{3+}. Suppression of T_{JT} by Ga substitution enables access to ferromagnetic ordering of the Mn spins in a phase having dynamic Jahn-Teller distortions. Comparison with the evolution of electronic properties in the single-valent family $RNiO_3$ (R denotes rare-earth metals, including yttrium) having a low-spin $t_{2g}^6 e_g^1$ electronic configuration on the Ni^{3+} ions highlights the role of the Hund intra-atomic-exchange coupling between the mobile e_g electrons and the localized spin $S=3/2$ of the t_{2g}^3 configuration on the Mn^{3+} ions, a coupling that prevents the e_g electrons from becoming delocalized in the paramagnetic state.

EXPERIMENTS AND RESULTS

Single crystals of $LnMnO_3$ (Ln=La, Pr, Nd, and Sm) were grown in an argon atmosphere from ceramic bars in an infrared-heating image furnace. The ceramic bars were prepared by solid-state reaction from the constituent oxides. A ceramic sample of $La_{0.5}Pr_{0.5}MnO_3$ was synthesized at 1250 °C and then annealed at 1000 °C in argon; the ceramic sample was used for measurement because a stable melting zone could not be achieved in an attempt to grow a $La_{0.5}Pr_{0.5}MnO_3$ crystal. The procedure for growing crystals of $LaMn_{1-x}Ga_xO_3$ has been reported elsewhere.[8] All samples were single phase as observed by x-ray powder diffraction and, as determined by the value of the thermoelectric power at room temperature, close to oxygen stoichiometry. Measurements of the transport properties were carried out in vacuum (10^{-3} atm) on a homemade setup as described elsewhere.[9] The contribution from the Pt leads was subtracted from the results. The dc magnetization was obtained with a SQUID magnetometer (Quantum Design).

Plots versus $1/T$ of the $\ln(\rho/T)$ and of the thermoelectric power $\alpha(T)$ for $LaMnO_3$ are superimposed in Fig. 1; they show clearly defined critical temperatures T^* and T_{JT}. The

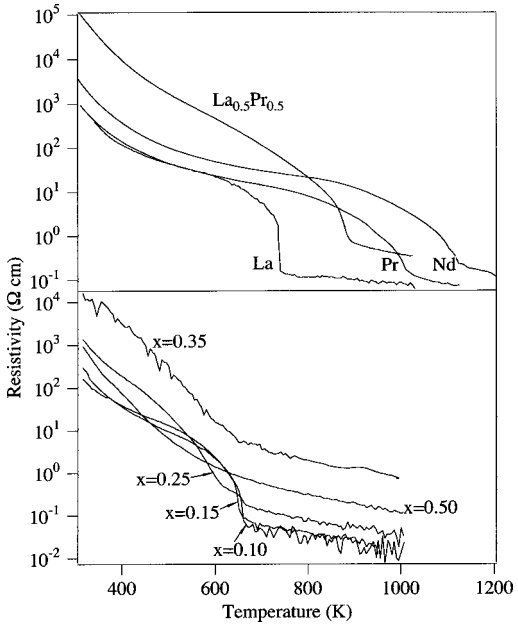

FIG. 2. Temperature dependence of the resistivity of (a) $LnMnO_3$ single-crystal samples with Ln=La, Pr, Nd and a ceramic sample with $Ln=La_{0.5}Pr_{0.5}$; (b) $LaMn_{1-x}Ga_xO_3$ ($0 \leqslant x \leqslant 0.5$). The much higher ρ in $Ln=La_{0.5}Pr_{0.5}$ appears to be due to heavy grain boundary scattering in this polycrystalline sample.

correspondence between T^* obtained from the change of slope of $\alpha(T)$ and a change from a linear dependence of $\ln(\rho/T)$ versus $1/T$ holds also for the other members of the $RMnO_3$ family and the system $LaMn_{1-x}Ga_xO_3$. The activation energy has been obtained from a linear fitting in a $\ln(\rho/T)$ versus $1/T$ plot and the temperature for this fitting is limited to the range where α changes gradually for $T<T^*$ and $T>T_{JT}$. The expression of $\rho=\rho_0 T\exp(E_a/kT)$ has been derived in the calculation of phonon-assisted hopping.[10] On the other hand, a $\ln\rho$ versus $1/T$ plot of our data gives a narrower range of linear temperature dependence than that obtained with the $\ln(\rho/T)$ versus $1/T$ plot. Although the O' to O^* transition at T_{JT} changes from first order to higher order with decreasing mean size of the A-site lanthanide ion in the $RMnO_3$ family, Fig. 2(a), and with increasing x in the $LaMn_{1-x}Ga_xO_3$ system, Fig. 2(b), nevertheless T_{JT} remains well defined in all samples but $x=0.50$. In all the samples, a large drop in ρ occurs in the interval $T^*<T<T_{JT}$; but the temperature dependence of the resistivity retains a semiconductive dependence with the intrinsic activation energy E_a given in Table I.

Table I also shows the E_a values obtained from $\ln(\rho/T)$ vs $1/T$ below T^* in the O' phase. Except for $LaMnO_3$ and $x=0.35$, the O^* phase has a higher apparent E_a than the O' phase below T^* even though its resistance is much lower. A reproducible room-temperature α before and after a high-temperature run rules out the possibility that the oxygen stoichiometry changes at $T>T_{JT}$. E_a in both the O' and O^* phases increases with decreasing size of the Ln^{3+} ion; it increases less with increasing x in the $LaMn_{1-x}Ga_xO_3$ system.

TABLE I. The activation energy obtained from the plot of $\ln(\rho/T)$ vs $1/T$ for $R\mathrm{MnO_3}$ and $\mathrm{LaMn_{1-x}Ga_xO_3}$. The error bar is ± 0.01 for those not labeled.

R or x	La	$\mathrm{La_{0.5}Pr_{0.5}}$[a]	Pr	Nd	0.1	0.15	0.25	0.35	0.5
E_a (eV) ($T<T^*$)	0.33	0.49	0.36	0.41	0.33	0.44	0.44	0.66 $\pm.03$	0.58 $\pm.03$
E_a (eV) ($T>T_{JT}$)	0.32	0.61	0.77 $\pm.07$	1.23 $\pm.07$	0.49 $\pm.03$	0.45	0.56	0.59	0.61

[a]Ceramic sample.

Figure 3 shows that the thermoelectric power $\alpha(T)$ for all samples, except $x=0.50$ of the $\mathrm{LaMn_{1-x}Ga_xO_3}$ system, exhibits a well-defined T^*. In the $R\mathrm{MnO_3}$ family, both T_{JT} and the interval $T^*<T<T_{JT}$ are seen to increase systematically with decreasing size of the A-site cation, i.e. with decreasing equilibrium (A-O) bond length and therefore with decreasing tolerance factor t. In the $\mathrm{LaMn_{1-x}Ga_xO_3}$ system, T^* and T_{JT} decrease with increasing x, but the interval $T^*<T<T_{JT}$ changes little with x.

DISCUSSION

The Mn-O-Mn overlap integral for the σ-bonding e_g orbitals is proportional to $\langle\cos\phi\rangle$, where ϕ is the bending of the $(180°-\phi)$ Mn-O-Mn bond angle resulting from the cooperative rotations of the $\mathrm{MnO_{6/2}}$ octahedra about a cubic [110] axis to accommodate a tolerance factor $t<1$.[11] The strength of the spin-spin interactions between localized-electron configurations is dominated by the σ-bond superexchange in the (001) planes and by semicovalent exchange along the c axis,[12] so a $T_N\sim\langle\cos^2\phi\rangle$ can be anticipated independent of whether the orbital ordering in the (001) planes is in phase or out of phase on traversing the c axis. Mizokawa *et al.*[13] have calculated that decreasing t stabilizes the in-phase arrangement.

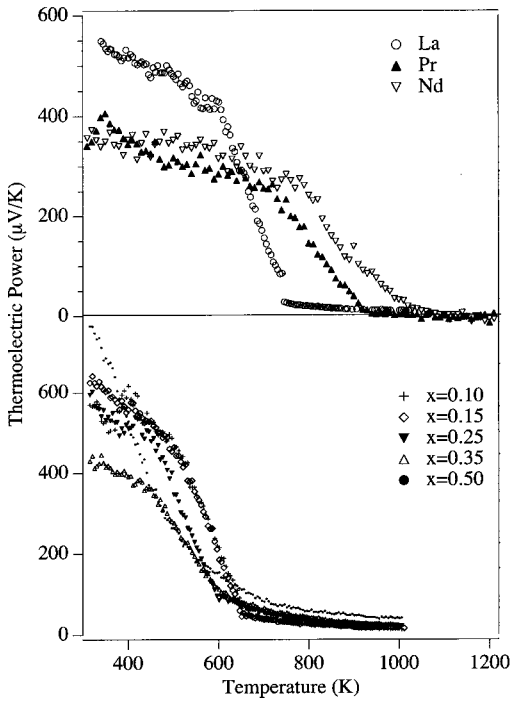

FIG. 3. Temperature dependence of the thermoelectric power on the same samples as Fig. 2.

We summarize our results in Fig. 4 where we plot for the $\mathrm{LnMnO_3}$ family not only T_N, but also T^* and T_{JT} versus $\langle\cos^2\phi\rangle$; for the $\mathrm{LaMn_{1-x}Ga_xO_3}$ system, we plot these critical temperatures versus x. A striking feature of Fig. 4 is the linear variations with $\langle\cos^2\phi\rangle$ or x of all three critical temperatures. Because T^* marks the onset of orbital-disorder fluctuations and T_{JT} the long-range orbital order-disorder transition, T^* can be expected to vary with $\langle\cos^2\phi\rangle$ in a manner similar to T_{JT}. A $T_N\sim\langle\cos^2\phi\rangle$ is due to a virtual charge transfer across the energy gap U between the $\mathrm{Mn^{4+}/Mn^{3+}}$ and $\mathrm{Mn^{3+}/Mn^{2+}}$ redox couples; perturbation theory introduces the square of an overlap integral. A linear decrease of T^* and T_{JT} with increasing $\langle\cos^2\phi\rangle$ means that the orbital-ordering temperature may be described as $T_{JT}\sim\alpha-\beta b^2/U$, where $b\sim\langle\cos\phi\rangle$ is the electron-energy transfer integral.

The existence of a disproportionation fluctuation on a fraction of the Mn atoms in the orbitally disordered phase shows that in the manganites having a redox-energy bandwidth W, the energy U separating the $\mathrm{Mn^{4+}/Mn^{3+}}$ and $\mathrm{Mn^{3+}/Mn^{2+}}$ couples decreases from a $U>W$ in the orbitally

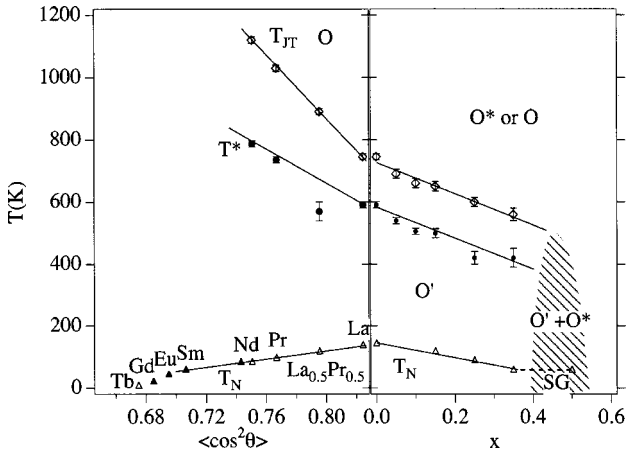

FIG. 4. Phase diagram of the transition temperatures as a function of $\langle\cos^2\phi\rangle$ and x for $\mathrm{LnMnO_3}$ and $\mathrm{LaMn_{1-x}Ga_xO_3}$. The anomalous value of T^* for $\mathrm{La_{0.5}Pr_{0.5}MnO_3}$ was obtained from a ceramic sample. The angle ϕ has been taken from the refinement from single-crystal diffraction (Refs. 25 and 26) and from powder diffraction (Ref. 27). The angle ϕ of $\mathrm{La_{0.5}Pr_{0.5}MnO_3}$ was taken as an average value of $\mathrm{LaMnO_3}$ and $\mathrm{PrMnO_3}$.

ordered phase to a finite $U<W$ in the orbitally disordered phase. The virtual charge transfers across the energy gap U in the orbitally ordered phase become real charge transfers in the orbitally disordered phase, and the associated breathing-mode oxide-ion displacements disrupt the cooperativity of the static Jahn-Teller deformations. The order parameter for the transition is the volume fraction of the orbitally ordered phase. In $LaMnO_3$, the order parameter drops discontinuously to zero in a first-order transition at T_{JT}; in $PrMnO_3$ and $NdMnO_3$ the transition is second order, and a nonpercolating volume of the ordered phase appears to persist above T_{JT} in analogy with a temperature range of short-range order.

Substitution of Ga^{3+} for Mn^{3+} in $LaMn_{1-x}Ga_xO_3$ weakens the cooperativity not only of the spin-spin interactions, but also of the Jahn-Teller distortions of the $MnO_{6/2}$ octahedral sites; therefore, T^* and T_{JT} decrease with increasing x in a manner similar to T_N. Nevertheless, a $T_{JT}\approx 580$ K is retained at $x=0.4$ whereas Figs. 2 and 3 provide no sharply defined T^* or T_{JT} at $x=0.5$. This disappearance of T^* and T_{JT} at high temperature is due to a spinodal phase separation. In the range $0.4<x\leqslant 0.5$, the system contains a ferromagnetic, orbitally disordered phase coexisting with an antiferromagnetic, orbitally ordered matrix.[8] X-ray diffraction from a powder obtained by crushing a small piece of the $x=0.5$ crystal showed retention of a matrix of the orbitally ordered O' phase at room temperature. The crystal was a magnetic glass in low magnetic fields; it converted to a ferromagnet with a complete spin-only magnetization in a field of 5 kOe, which reveals the presence of a ferromagnetic, orbitally disordered minority phase that grows in an applied magnetic field at the expense of the orbitally ordered antiferromagnetic matrix. Note that the $x=0.5$ sample is an insulator; double exchange is not operative and the ferromagnetic coupling associated with orbital fluctuations demonstrates the existence of the ferromagnetic vibronic-superexchange interaction proposed years ago.[14] Figures 2 and 3 show that the transport properties of the $x=0.5$ crystal vary smoothly over the entire temperature range of measurement; no well-defined change of slope in either $\rho(T)$ or $\alpha(T)$ is found to signal either T^* or T_{JT} of a percolating matrix, perhaps because the orbitally ordered matrix does not percolate until temperatures well below T_{JT}.

At temperatures $T<T^*$, the activation energies E_a in Table I of $\rho/T\sim\exp(-E_a/kT)$ reflect the motional enthalpy ΔH_m of a small-polaron mobility. In the case of $LaMnO_3$, $E_a\approx\Delta H_m\approx 0.33$ eV for $T<T^*$ is essentially the same, 0.32 eV, for $T>T_{JT}$. $E_a=0.33$ eV for $T<T^*$ is close to the energy of the leading edge of the gap E_g in optical conductivity.[7] Closing up of this E_g at $T>T_{JT}$ (Ref. 7) indicates that more charge carriers are available and the activation energy obtained in this temperature range also reflects the motional enthalpy ΔH_m. This observation implies that the bond-length fluctuations perturb the periodic potential so as to introduce Anderson localized states in band tails that overlap at $T>T_{JT}$. Although U is reduced, the energy gap between mobility edge remains huge. What limits the volume fraction of disproportionation fluctuations in the O^* phase above T_{JT} appears to be retention of a finite $U<W$. Table I shows that $E_a\approx\Delta H_m$ for $T<T^*$ increases progressively as the size of the lanthanide ion decreases, i.e., as the tolerance factor t decreases. (The variance of the A-site cation sizes in the ceramic $La_{0.5}Pr_{0.5}MnO_3$ sample may influence its E_a value). For $T>T_{JT}$, the larger value of E_a in $PrMnO_3$ and $NdMnO_3$ than that for $T<T^*$ implies $E_a\approx\Delta H_m+(E_g/2)$ in the temperature range $T>T_{JT}$ of measurement; E_g would be the energy required to create additional disproportionation fluctuations.

We note that the structure above T_{JT} changes from pseudocubic O^* with $c/a\approx\sqrt{2}$ to O orthorhombic with $c/a>\sqrt{2}$ on passing from $LaMnO_3$ to $PrMnO_3$ and $NdMnO_3$ (Ref. 15) and that the transition at T_{JT} changes from first to second order as T_{JT} increases. The short temperature interval of measurement above T_{JT} in the case of $PrMnO_3$ and $NdMnO_3$ may represent a smooth decrease in the volume fraction of the orbitally ordered phase above T_{JT}, this fraction disappearing at higher temperatures. In the $LaMn_{1-x}Ga_xO_3$ system, the activation energies $E_a\approx\Delta H_m$ remain similar for $T<T^*$ and $T>T_{JT}$, but ΔH_m increases with x as the number of Mn near neighbors decreases.

The orbital ordering below T_{JT} in $LaMnO_3$ introduces anisotropic spin-spin interactions that result in type-A magnetic order below the Néel temperature T_N.[1] This type-A magnetic order is found for all the $RMnO_3$ compounds of this study, i.e., for Ln=La, $La_{0.5}Pr_{0.5}$, Pr, and Nd. However, a helical spin configuration has been found in $TbMnO_3$,[16] and a type-E spin configuration in $HoMnO_3$ consists of an unusual up-up-down-down spin ordering on successive (111) planes.[17] Given an increase in the splitting U between the Mn^{4+}/Mn^{3+} and Mn^{3+}/Mn^{2+} couples as the tolerance factor $t<1$ decreases, these changes in the long-range magnetic order appear to reflect an increase in the next-near-neighbor spin-spin interactions as the $(180°-\phi)$ Mn-O-Mn bond angle decreases.[18]

In an oxide, octahedral-site Ni^{3+} has the low-spin configuration $t_{2g}^6e_g^1$ with a single e_g electron in a twofold orbital degeneracy; it is, therefore, a Jahn-Teller ion such as high-spin Mn^{3+}: $t_{2g}^3e_g^1$, but without the strong Hund intra-atomic-exchange coupling of the e_g electron to a localized spin $S=3/2$ from a half-filled t_{2g}^3 manifold. Therefore, it is instructive to compare the phase diagram of Fig. 5 for the $RNiO_3$ family with that of Fig. 4 for the $RMnO_3$ family.

The O'-O^* orthorhombic transition at T_{JT} in Fig. 4 is replaced in Fig. 5 by an insulator-metal transition at T_{IM} from monoclinic ($P2_1/n$) to orthorhombic symmetry; the magnetic order below T_N is type E in Fig. 5, whereas it is type A in Fig. 4 for the lighter lanthanides of $RMnO_3$. The relation $T_N\sim\langle\cos^2\phi\rangle$ holds in the $RNiO_3$ family only until it is intercepted by T_{IM} in the system $Nd_{1-x}Sm_xNiO_3$ at $x\approx 0.4$. Okazaki *et al.*[19] have studied the $Nd_{1-x}Sm_xNiO_3$ system with photoemission spectroscopy and have found the appearance of a pseudogap in the metallic phase above T_{IM} for $x>0.4$. We have shown elsewhere[20] evidence for the coexistence of strong-correlation fluctuations in a metallic matrix already in $LaNiO_3$, the volume fraction of these fluctuations increasing as T_{IM} increases, and we have found the

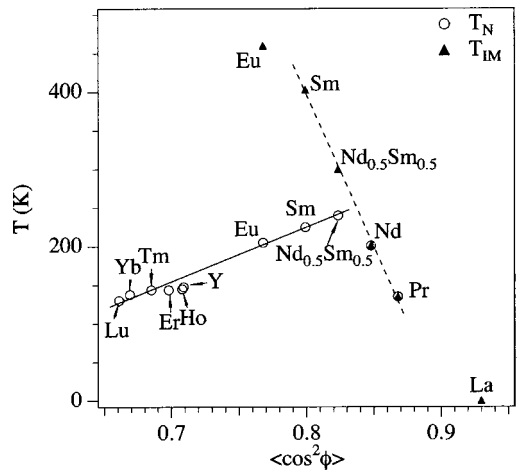

FIG. 5. The phase diagram of $R\mathrm{NiO_3}$ (R=La, Pr, Nd, Sm, Eu, and Gd). The transition temperatures have been taken from Ref. 28 and the angle ϕ from Ref. 29.

associated bond-length fluctuations in the vicinity of T_{IM} in Fig. 5 where a crossover from localized to itinerant electronic behavior occurs.[21]

Measurement of the change of T_{N} with hydrostatic pressure has shown that the assumption of a pressure-independent electron-transfer energy gap in the superexchange perturbation theory breaks down in $\mathrm{LaMnO_3}$;[22] a similar conclusion has been obtained for $\mathrm{SmNiO_3}$.[21] As far as we know, clear evidence of orbital ordering in the monoclinic phase below T_{IM} has not been reported. However, it has been argued[23] that the two distinguishable Ni sites refined in $P2_1/n$ may be explained by different orbital orderings instead of a small charge disproportionation as determined by other groups.[24] The difference between Figs. 4 and 5 reflect a greater degree of delocalization of the e_g electrons in the $R\mathrm{NiO_3}$ family than in the $R\mathrm{MnO_3}$ family. Two factors contribute to this difference: (1) the Hund intra-atomic-exchange coupling on a $\mathrm{Mn^{3+}}$ ion, which is not present on a low-spin $\mathrm{Ni^{3+}}$ ion, and (2) a stronger O $2p$ component in the e_g orbitals of $\mathrm{Ni^{3+}}$ than those of $\mathrm{Mn^{3+}}$ because the $\mathrm{Ni^{3+}/Ni^{2+}}$ redox couple is pinned at the top of the O $2p$ bands, whereas an on-site Coulomb energy U separates the $\mathrm{Mn^{4+}/Mn^{3+}}$ couple from the $\mathrm{Mn^{3+}/Mn^{2+}}$ couple.

Consequently, the characters of the two low-temperature insulator phases are different; the manganese oxides have an O' orthorhombic structure and require a quite small tolerance factor to stabilize type-E antiferromagnetic order, whereas the nickel oxides have a type-E magnetic order below T_{N} for all compositions and a monoclinic ($P2_1/n$) symmetry with two distinguishable $\mathrm{Ni^{3+}}$ sites having different mean (Ni-O) bond lengths. Spin-spin coupling to next-near neighbors in the $R\mathrm{NiO_3}$ family is due to a larger O $2p$ component in the e_g orbitals as well as a small tolerance factor. On the other hand, the conductive phases above T_{JT} and T_{IM} appear to be similar; in both families, the conductive phases have properties characteristic of the coexistence of itinerant and localized electronic states although the manganites exhibit an activated electronic mobility and the nickelates change from metallic to vibronic behavior as T_{IM} increases with decreasing tolerance factor. Moreover, the transitions at T_{IM} and at T_{JT} both change from first order to higher order as the tolerance factor decreases in the localized-electron domain.

CONCLUSIONS

Measurements on single crystals of the high-temperature transport properties and the low-temperature magnetic properties of the $R\mathrm{MnO_3}$ (R=La, Pr, Nd) family and the $\mathrm{LaMn_{1-x}Ga_xO_3}$ system with $0 \leqslant x \leqslant 0.5$ have revealed the following: (1) An orbital order-disorder transition occurring over a temperature interval $T^* < T < T_{\mathrm{JT}}$ is associated with marked changes of resistivity and thermoelectric power as well as a structural transition from O' orthorhombic in the orbitally ordered phase to O^* or O orthorhombic in the orbitally disordered phase. (2) Collapse of the thermoelectric power over the interval $T^* < T < T_{\mathrm{JT}}$ shows a disproportionation reaction occurs on a fraction of the Mn atoms in the orbitally disordered phase, but a finite $U < W$ is retained. (3) The mobility of the electronic charge carriers remains activated in the orbitally disordered phase with a motional enthalpy ΔH_m similar to the activation energy E_a in the orbitally ordered phase. (4) In $\mathrm{LaMnO_3}$, the volume fraction of Mn atoms undergoing disproportionation fluctuations remains unchanged above a first-order transition from the O' to the O orthorhombic structure at T_{JT}; the finite $U < W$ does not change with increasing temperature. (5) In the $R\mathrm{MnO_3}$ family, T^* and T_{JT} vary linearly with $\langle \cos^2 \phi \rangle$ as does T_{N}; the angle ϕ measures the bending of the $(180° - \phi)$ Mn-O-Mn bond angle, and a virtual charge transfer from one atom to a neighbor varies, in second-order perturbation theory, as $\langle \cos^2 \phi \rangle$. T^* and T_{JT} decrease with increasing virtual charge transfer whereas T_{N} increases. (6) T^*, T_{JT}, and T_{N} all decrease linearly with x in $\mathrm{LaMn_{1-x}Ga_xO_3}$ for $0 \leqslant x \leqslant 0.4$, but T^* and T_{JT} are not defined by the transport data in the $x = 0.5$ sample where spin-glass and metamagnetic behavior signal the coexistence of an orbitally ordered, antiferromagnetic phase and an orbitally disordered ferromagnetic phase in low magnetic fields; the ferromagnetic phase grows in an external magnetic field. (7) Comparison of the phase diagrams for the $R\mathrm{MnO_3}$ and $R\mathrm{NiO_3}$ families shows that these single-e_g-electron systems exhibit common features on the approach, from the localized-electron side, to crossover from localized to itinerant electronic behavior. However, the Hund intra-atomic exchange and a smaller O $2p$ component in the e_g orbitals of the $\mathrm{Mn^{3+}}$ ions restrict the $R\mathrm{MnO_3}$ family to localized-electron behavior, whereas the $R\mathrm{NiO_3}$ family undergoes crossover to itinerant-electron behavior on passing from $\mathrm{SmNiO_3}$ to $\mathrm{LaNiO_3}$.

ACKNOWLEDGMENTS

The authors would like to thank the NSF, the TCSUH of Houston, Texas, and the Robert A. Welch Foundation of Houston, Texas for financial support.

[1] J. B. Goodenough, Phys. Rev. **100**, 564 (1955).
[2] J. Rodriguez-Carvajal, M. Hennion, F. Moussa, A. H. Moudden, L. Pinsard, and A. Revcolevschi, Phys. Rev. B **57**, R3189 (1998).
[3] J.-S. Zhou and J. B. Goodenough, Phys. Rev. B **60**, R15002 (1999).
[4] E. Granado, J. A. Sanjurjo, C. Rettori, J. J. Neumeier, and S. B. Oseroff, Phys. Rev. B **62**, 11 304 (2000).
[5] L. Martin-Carron, Eur. Phys. J. B **22**, 11 (2001).
[6] M. C. Sanchez, G. Subias, J. Garcia, and J. Blasco, Phys. Rev. Lett. **90**, 045503 (2003).
[7] K. Tobe, T. Kimura, Y. Okimmoto, and Y. Tokura, Phys. Rev. B **64**, 184421 (2001).
[8] J.-S. Zhou and J. B. Goodenough, Phys. Rev. B **63**, 184423 (2001).
[9] J.-S. Zhou and J. B. Goodenough, Phys. Rev. B **54**, 13 393 (1996).
[10] D. Emin and T. Holstein, Ann. Phys. (N.Y.) **53**, 439 (1969).
[11] C. Boekema, F. Van Der Woude, and G. A. Sawatzky, Int. J. Magn. **3**, 341 (1972).
[12] J.-S. Zhou and J. B. Goodenough, Phys. Rev. B **68**, 054403 (2003).
[13] T. Mizokawa, D. I. Khomskii, and G. A. Sawatzky, Phys. Rev. B **60**, 7309 (1999).
[14] J. B. Goodenough, A. Wold, R. J. Arnott, and N. Menyuk, Phys. Rev. **124**, 373 (1961).
[15] D. Sanchez, J. A. Alonso, and M. J. Martinez-Lope, J. Chem. Soc. Dalton Trans. **2002**, 4422.
[16] J. Blasco, C. Ritter, J. Garcia, J. M. de Teresa, J. Perez-Cacho, and M. R. Ibarra, Phys. Rev. B **62**, 5609 (2000).
[17] A. Munoz, M. T. Casais, J. A. Alonso, M. J. Martinez-Lope, J. L. Martinez, and M. T. Fernandez-Diaz, Inorg. Chem. **40**, 1020 (2001).
[18] T. Kimura, S. Ishihara, K. T. Takahashi, H. Shintani, and Y. Tokura, cond-mat/0211568v1 (unpublished).
[19] K. Okazaki, T. Mizokawa, A. Fujimori, E. V. Sampath Kumaran, M. T. Martinez-Lope, and J. A. Alonso, Phys. Rev. B **67**, 073101 (2003).
[20] J.-S. Zhou, J. B. Goodenough, B. Dabrowski, P. W. Klamut, and Z. Bukowski, Phys. Rev. B **61**, 4401 (2000).
[21] J.-S. Zhou, J. B. Goodenough, and B. Dabrowski, Phys. Rev. B **67**, 020404(R) (2003).
[22] J.-S. Zhou and J. B. Goodenough, Phys. Rev. Lett. **89**, 087201 (2002).
[23] J. Rodriguez-Carvajal, S. Rosenkranz, M. Medarde, P. Lacorre, M. T. Fernandez-Diaz, F. Fauth, and V. Trounov, Phys. Rev. B **57**, 456 (1998).
[24] J. A. Alonso, J. L. Garcia-Munoz, M. T. Fernandez-Diaz, M. A. G. Aranda, M. J. Martinez-Lope, and M. T. Casais, Phys. Rev. Lett. **82**, 3871 (1999).
[25] T. Mori, K. Aoki, N. Kamagashira, T. Shishido, and T. Fukuda, Mater. Lett. **42**, 387 (2000).
[26] T. Mori, N. Kamagashira, K. Aoki, T. Shishido, and T. Fkuda, Mater. Lett. **54**, 238 (2002).
[27] J. A. Alonso, M. J. Martinez-Lope, M. T. Casais, and M. T. Fernandez-Diaz, Inorg. Chem. **39**, 917 (2000).
[28] J. B. Torrance, P. Lacorre, A. I. Nazzal, E. J. Ansaldo, and Ch. Niedermayer, Phys. Rev. B **45**, 8209 (1992).
[29] J. A. Alonso, M. J. Martinez-Lope, M. T. Casais, J. L. Garcia-Munoz, and M. T. Fernandez-Diaz, Phys. Rev. B **61**, 1756 (2000).